Cell Reports

Astrocytes and oligodendrocytes in the thalamus jointly maintain synaptic activity by supplying metabolites

Graphical abstract

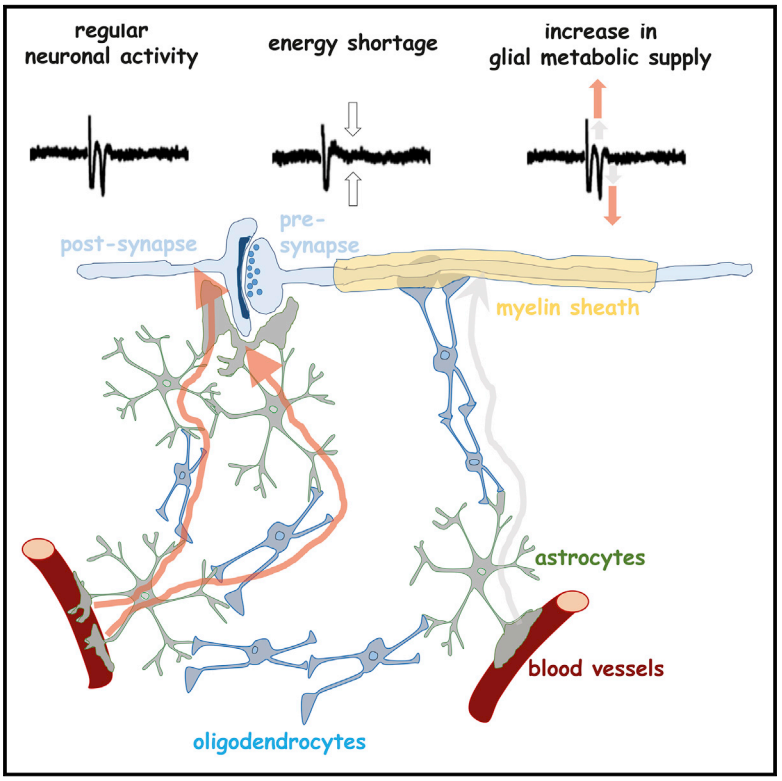

Highlights

- In the thalamus, astrocytes and oligodendrocytes form large coupled networks
- These panglial networks are essential for energy supply to neurons
- Oligodendrocytes assist astrocytes in metabolite transfer to postsynapses

Authors

Camille Philippot, Stephanie Griemsmann, Ronald Jabs, Gerald Seifert, Helmut Kettenmann, Christian Steinhäuser

Correspondence

cste@uni-bonn.de

In Brief

Philippot et al. show that, in the thalamus, astrocytes and oligodendrocytes form large-gap junction-coupled networks, which are required to deliver energy substrates for sustaining neuronal activity. The role of oligodendrocytes in these networks is not to provide nutrients to axons but to assist astrocytes in metabolite transfer to postsynapses.

Philippot et al., 2021, Cell Reports *34*, 108642
January 19, 2021
https://doi.org/10.1016/j.celrep.2020.108642

CellPress

Cell Reports

CellPress
OPEN ACCESS

Report

Astrocytes and oligodendrocytes in the thalamus jointly maintain synaptic activity by supplying metabolites

Camille Philippot,[1] Stephanie Griemsmann,[1] Ronald Jabs,[1] Gerald Seifert,[1] Helmut Kettenmann,[2] and Christian Steinhäuser[1,3,*]

[1]Institute of Cellular Neurosciences, Medical Faculty, University of Bonn, Venusberg-Campus 1, 53127 Bonn, Germany
[2]Cellular Neurosciences, Max Delbrück Center for Molecular Medicine in the Helmholtz Association, Robert Roessle Str. 10, 13125 Berlin, Germany
[3]Lead Contact
*Correspondence: cste@uni-bonn.de
https://doi.org/10.1016/j.celrep.2020.108642

SUMMARY

Thalamic astrocytes and oligodendrocytes are coupled via gap junctions and form panglial networks. Here, we show that these networks have a key role in energy supply of neurons. Filling an astrocyte or an oligodendrocyte in acute slices with glucose or lactate is sufficient to rescue the decline of stimulation-induced field post-synaptic potential (fPSP) amplitudes during extracellular glucose deprivation (EGD). In mice lacking oligodendroglial coupling, loading an astrocyte with glucose does not rescue the EGD-mediated loss of fPSPs. Monocarboxylate and glucose transporters are required for rescuing synaptic activity during EGD. In mice deficient in astrocyte coupling, filling of an oligodendrocyte with glucose does not rescue fPSPs during EGD. Our results demonstrate that, in the thalamus, astrocytes and oligodendrocytes are jointly engaged in delivering energy substrates for sustaining neuronal activity and suggest that oligodendrocytes exert their effect mainly by assisting astrocytes in metabolite transfer to the postsynapse.

INTRODUCTION

Glial cells are key elements to guarantee proper brain function by providing energy substrates to neurons. Astrocytic endfeet are strategically located in close contact to blood vessels and cover a large part of their surfaces. Astrocytes, as well as capillary endothelial cells, express the glucose transporter, GLUT1, which allows astrocytes to take up glucose from the circulation (Bélanger et al., 2011). Glucose is then metabolized to lactate by glycolysis. Described by Pellerin and Magistretti (1994) as the astrocyte-neuron lactate shuttle (ANLS), astrocyte-derived lactate is then transported to the synapse, via monocarboxylate transporters (mainly MCT4 in astrocytes and MCT2 in neurons), to fuel neurons (Pellerin and Magistretti, 1994). In addition, glycogen, which is almost exclusively localized to astrocytes, serves as a significant energy reserve for the brain. Glycogen breakdown also results in lactate production, is released in the extracellular space, and is taken up by neurons to fuel their energy needs (Magistretti et al., 1993; Bélanger et al., 2011). Rouach et al. (2008) demonstrated that, in the hippocampus, delivery of glucose or lactate from astrocytes is needed to maintain neuronal synaptic transmission during extracellular glucose deprivation (Rouach et al., 2008). Gap junction coupling among astrocytes is required for this protective effect. Gap junctions are formed by connexin proteins (Cx), which are expressed in a cell-type-specific manner (Goodenough et al., 1996; Bedner et al., 2012). They allow intercellular exchange through diffusion of small molecules, such as ions, second messengers, and energy metabolites, including glucose and lactate (Giaume et al., 2010).

The thalamus has been described as the gate to consciousness (Crick and Koch, 2003) because it has a key role in relay and modulation of sensory and motors signals to the neocortex (Sherman and Guillery, 2002) as well as in the generation of sleep-related rhythms (Crunelli and Hughes, 2010). In the thalamus, unlike the neocortex or the hippocampus, many astrocytes lack Cx43 but, instead, abundantly express Cx30 (Griemsmann et al., 2015). Oligodendrocytes mainly express the Cx isoforms Cx32 and Cx47. Tracer filling of individual thalamic glial cells revealed abundant astrocyte-oligodendrocyte coupling, called panglial coupling. This is different from other brain regions, e.g., the hippocampus and the neocortex, in which panglial coupling is much less prevalent (Griemsmann et al., 2015). The functional effect of oligodendrocytes within these gray matter panglial networks is still unclear. It has been shown that, in white matter, networks of coupled oligodendrocytes support the axonal function by transport of metabolites (Lee et al., 2012; Meyer et al., 2018). Thus, because oligodendrocytes are not in direct contact with blood vessels, panglial coupling in the thalamus might be needed to transport energy metabolites from the circulation, via astrocytes and oligodendrocytes, to synaptic structures and/or to axons. Here, we assessed

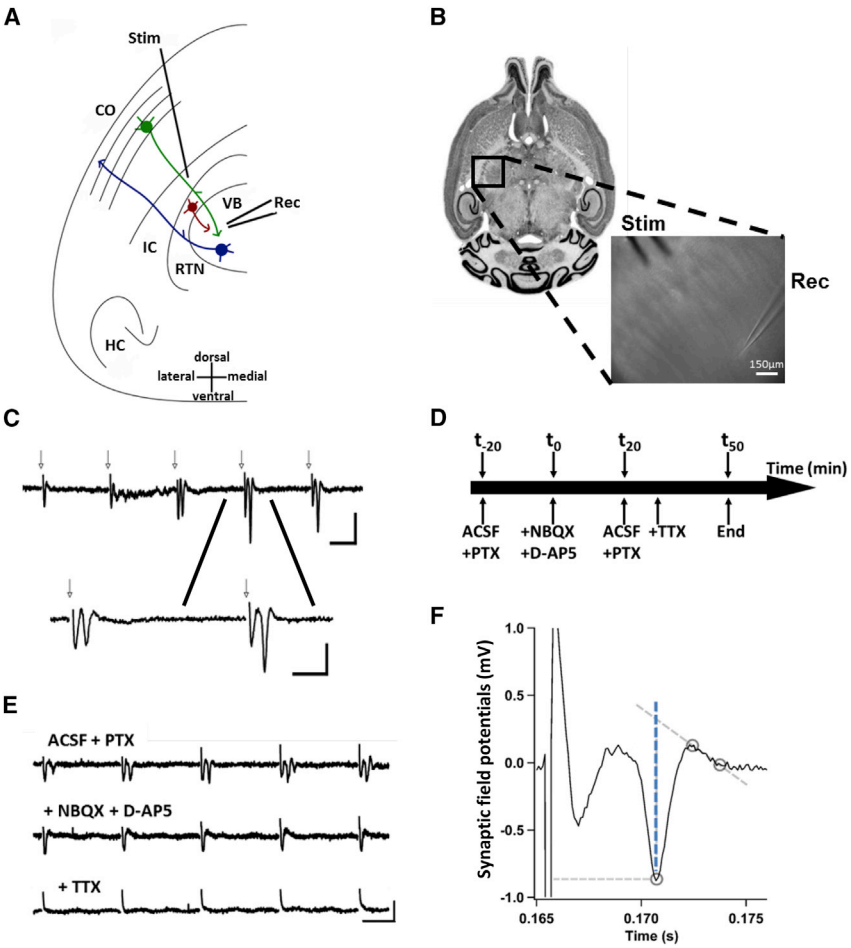

Figure 1. Slice preparation and evaluation of fPSPs

(A) Scheme of a coronal section of a mouse brain containing cortex (CO), internal capsule (IC), reticular thalamic nucleus (RTN), and ventrobasal thalamus (VB). In addition, the hippocampus (HC) is displayed, and the cross indicates slice orientation (bottom). The cortico-thalamic pathway is indicated by a green neuron, the thalamo-cortical pathway is shown in blue, and a GABAergic neuron of the RTN is displayed in brown. Stim, stimulation electrode; Rec, recording electrode. Modified from (Grant et al., 2012).

(B) Slice used for recordings; inset shows stimulation and field recording electrodes.

(C) Stimulation trains of five pulses (indicated by arrows) were applied and repeated every 15 s. The depicted averages of 10 successive traces were used for analysis. Scale bar, 20 ms, 0.5 mV. A blow-up of the fourth response is shown. Scale bar, 10 ms, 0.5 mV.

(D) Timeline of the experimental protocols.

(E) fPSPs were sensitive to blockers of ionotropic glutamate receptors (middle trace) but not $GABA_A$ receptors (top). The bottom trace shows a recording after TTX application (residual signals are stimulation artifacts). Scale bar, 20 ms, 0.2 mV.

(F) Scheme depicting fPSP analysis by a custom-made Igor Pro tool, by placing three measuring points on the trace (gray circles). fPSP amplitude (blue dotted line) was determined as the distance between the intersection of the tangent and the minimum of the second negative deflection.

whether, and through which mechanisms, oligodendrocytes in the thalamus are participating in the energy provision of neurons. By stimulating the cortico-thalamic pathway, we found that extracellular glucose deprivation (EGD) suppresses thalamic post-synaptic field potentials (fPSPs), which could not be rescued by extracellular lactate or pyruvate. Importantly, the loss of fPSPs during EGD was fully prevented when filling an individual astrocyte with glucose or lactate, a process that required glucose and monocarboxylate transporter activity. Filling of individual oligodendrocyte with glucose also rescued fPSPs during EGD. Thus, in the thalamus, astrocytes and oligodendrocytes are jointly engaged in maintaining synaptic activity by delivery of metabolites through the panglial coupling network.

RESULTS

Characterization of post-synaptic field potentials in the ventrobasal thalamus

To record thalamic fPSPs, coronal brain slices with a 30° angle to the horizontal plane were prepared. A bipolar stimulation electrode was placed into the internal capsule, and the field recording electrode was located at the ventrobasal thalamus (Figures 1A and 1B). Stimulation of the cortico-thalamic pathway (indicated by the green neuron in Figure 1A; five pulses, 100 µs at 20 Hz, every 15 s) in the presence of picrotoxin (100 µM), to block GABAergic neurons of the reticular thalamic nucleus (RTN), evoked fPSPs (Figures 1C–1F). The stimulation intensity was set to elicit 80% of the maximal responses. This protocol allowed for long-term monitoring (>1 h) of synaptic activity without inducing long-term potentiation (LTP) or long-term depression (LTD). fPSPs were isolated by subtracting responses evoked in the presence of picrotoxin, D-AP5, and NBQX from responses in artificial cerebrospinal fluid (ACSF) (Figures 1C and 1D). Thalamic fPSPs were completely blocked by adding tetrodotoxin (TTX) (0.5 µM) to the bath solution (Figure 1E, bottom). fPSP amplitudes were calculated as the voltage difference between the second peak (minimum) of the field potential and the intersection of its extrapolated slope (dotted lines in Figure 1F).

EGD leads to a rapid decline of thalamic fPSPs and cannot be rescued by bath application of lactate or pyruvate

In ACSF containing 11 mM of glucose, stable fPSPs could be recorded over >40 min (Figures 2A and 2B, black line, and

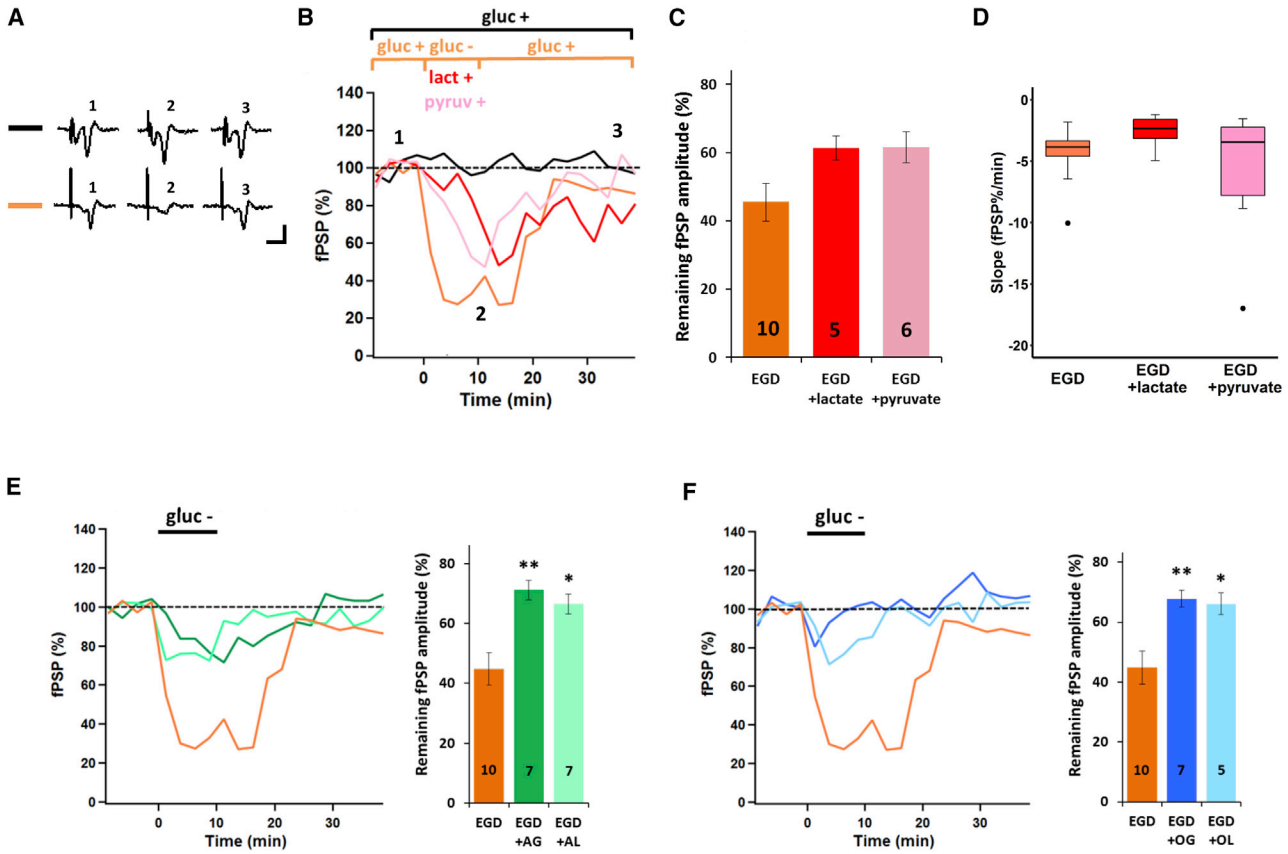

Figure 2. EGD-induced depression of thalamic fPSPs is Rescued by glucose or lactate filling of an astrocyte or oligodendrocyte

(A) Example traces of thalamic field potentials in slices from hGFAP-EGFP mice. Top: control recordings, indicated by black lines in (B), with numbers corresponding to time points indicated in (B). Bottom: recordings obtained (1) before removal of extracellular glucose, (2) during EGD, and (3) after reperfusion with glucose-containing bath solution, indicated by the orange lines in (B). Scale bars, 0.5 ms, 0.5 mV.

(B) Representative traces of thalamic fPSPs under control conditions (gluc$^+$, black lines) and during a 10 min of EGD (gluc$^-$, EGD, orange; n = 12, N = 10). Red and pink curves represent fPSPs in which extracellular glucose was replaced by L-lactate (22 mM; n = 9, N = 5) or by pyruvate (22 mM, n = 6, N = 6), respectively.

(C) Bar graphs represent the means and SEM of the remaining fPSP amplitudes, normalized to the respective condition before EGD. Extracellular lactate and pyruvate did not rescue the EGD-induced decline of fPSPs. Number of mice is given in the bar graphs.

(D) Boxplots represent the median of the slope (fPSP%/min) of the respective condition using linear approximation and comparing the steepness of the curves. Extracellular lactate and pyruvate did not affect fPSP slope compared with the EGD-only experiments.

(E) Representative traces of fPSPs during EGD (EGD, orange, n = 12, N = 10; same EGD trace is shown for comparison in Figures 2, 3, and 4), during EGD after filling an hGFAP-EGFP-positive astrocyte with glucose (20 mM, EGD+AG, dark green; n = 8, N = 7) and during EGD after filling an astrocyte with L-lactate (40 mM, EGD+AL, light green; n = 7, N = 6). The bar graphs (right) compare the amplitudes of the fPSPs remaining under the respective conditions, normalized to amplitudes before EGD. Astrocytes loaded with glucose or lactate could partially rescue thalamic fPSP amplitudes during EGD. Error bars represent SEM.

(F) Representative recordings of fPSPs during EGD (EGD, orange, n = 12, N = 10), during EGD after filling a PLP-GFP-positive oligodendrocyte with glucose (20 mM, EGD+OG, dark blue; n = 9, N = 7), and during EGD after filling an oligodendrocyte with L-lactate (40 mM, EGD+OL, light blue; n = 5, N = 5). The histogram (right) compares the fPSPs remaining under the respective conditions, normalized to the amplitudes before EGD. Loading of oligodendrocytes with glucose or lactate partially rescued fPSPs during EGD. The number of mice is given in the bar graphs. ANOVA followed by Tukey's post hoc-test. *$p < 0.05$, **$p < 0.01$. Error bars represent SEM.

Figure 1). For EGD experiments, first, control fPSPs were recorded in ACSF (10 min); then, glucose was removed from the bath (10 min; gluc-), and subsequently, ACSF was reperfused (30 min). During EGD, fPSPs declined to around 45% of the initial amplitude and recovered upon reperfusion with ACSF (Figure 2, orange line and bar graph). Similar to the corpus callosum (Meyer et al., 2018), extracellular replacement of glucose with equistoichiometric amounts of L-lactate (22 mM, n = 5) or pyruvate (22 mM, N = 6) did not rescue the transient decline of fPSPs, with the drop to about 60% of the control value being not statistically different from that observed in ACSF lacking glucose (Figures 2B and 2C; p = 0.13 and 0.10 for L-lactate and pyruvate, respectively). Reperfusion of glucose after lactate or pyruvate application led to a similar recovery of fPSPs as that observed after EGD. The kinetics of the fPSP decline was analyzed using linear approximation of the decay and comparing the slopes. There was no significant difference when comparing the EGD-only condition with the EGD + lactate and EGD + pyruvate conditions (Figure 2D; p = 0.307, Kruskal-Wallis).

The decline of fPSPs during EGD can be rescued by filling an astrocyte with glucose or lactate

We investigated whether, in the thalamus, metabolite loading of glial cells counterbalances the EGD-mediated loss of fPSP amplitudes. Astrocytes were identified by employing acute brain slices from hGFAP-GFAP mice. Although thalamic astrocytes are almost devoid of GFAP protein, many of them express hGFAP promoter activity and can be identified by their intrinsic fluorescence and morphology (Griemsmann et al., 2015; Matthias et al., 2003). An astrocyte was patched and filled through the pipette solution with a high concentration of glucose (20 mM, 20 min). Subsequently, EGD was performed (10 min), followed by reperfusion of the ACSF. The pipette solution also contained the gap-junction-permeable dye sulforhodamine-B to monitor a successful spread into the coupled networks. The patched cells displayed electrophysiological properties typical of astrocytes, including a very low input resistance (2.9 ± 0.3 MΩ; n = 15, N = 14). Glucose filling of an astrocyte significantly reduced the EGD-dependent drop of fPSPs (control EGD, same as in Figure 2C, to 45 ± 5%, N = 10; after astrocyte filling, to 71 ± 5.5%; N = 7; p = 0.004) (Figure 2E). We also tested whether filling of astrocytes with L-lactate (40 mM, N = 6, because during lactic fermentation 1 molecule of glucose generates 2 molecules of lactate) can rescue fPSP. Indeed, under this condition, the EGD-induced drop of fPSPs was also reduced (to 66 ± 3.26%; n = 6, p = 0.014) (Figure 2E). In conclusion, high glucose or L-lactate filling of astrocytes can rescue the decline of fPSP amplitudes during EGD in the thalamus.

Filling an oligodendrocyte with glucose or lactate also rescues fPSPs during EGD in the thalamus

We have previously reported that, in the thalamus, astrocytes and oligodendrocytes form abundant panglial coupling networks (Griemsmann et al., 2015; Claus et al., 2018). In the corpus callosum, Meyer et al. (2018) demonstrated a critical role for oligodendrocytes, rather than astrocytes, in coupling-dependent provision of energy substrates to prevent the decline of axonal activity during EGD. To test whether oligodendrocytes similarly protect synaptic activity in the thalamus, individual oligodendrocytes of PLP-GFP mice were filled with glucose (20 mM) or lactate (40 mM), and fPSPs were recorded as described above. The input resistance of the cells was 7.7 ± 4.1 MΩ (n = 13, N = 12). Similar to dialyzing astrocytes with energy metabolites, loading of oligodendrocytes with high glucose concentration (20 mM, N = 7) significantly reduced the decline of fPSPs during EGD (to 68 ± 3%, p = 0.01). Loading an oligodendrocyte with lactate (40 mM, N = 5) had a comparable effect (decline to 66 ± 4%, p = 0.031) (Figure 2F). In conclusion, filling of individual astrocytes or oligodendrocytes with energy substrates is equally efficient at attenuating EGD-induced impairment of fPSP activity in the thalamus.

The protective effect of astrocyte glucose filling on fPSP activity requires astrocyte-oligodendrocyte gap junction coupling

In the thalamus, Cx30 is the dominating astrocytic connexin, and astrocyte-oligodendrocyte coupling is mainly mediated by heterotypic Cx32:Cx30 channels (Griemsmann et al., 2015; Claus et al., 2018). To investigate the putative effect of oligodendrocyte coupling on energy substrate provision, we first investigated the coupling efficiency by filling a thalamic astrocyte in $Cx32^{-/-}$;$Cx47^{EGFP(-/-)}$ (dko) (n = 10, N = 3), $Cx32^{-/-}$;$Cx47^{EGFP(+/-)}$ (n = 11, N = 4) and $Cx32^{-/-}$;$Cx47^{+/+}$ mice (n = 15, N = 4) with biocytin (during 20 min of patch clamp recording; Figures 3A and 3C). Coupling efficiency was significantly reduced in dko mice (36 ± 8 cells, n = 10 slices), compared with that of $Cx32^{-/-}$;$Cx47^{EGFP(+/-)}$ mice (69 ± 11 cells, n = 11 slices, p = 0.048) (Figure 3A) and of control mice (110 ± 20 cells from PLP-GFP mice, p = 0.0028; (Griemsmann et al., 2015), whereas it did not differ from $Cx32^{-/-}$;$Cx47^{+/+}$ mice (58 ± 2 cells, n = 15 slices, p = 0.12). Furthermore, in the $Cx32^{-/-}$;$Cx47^{EGFP(+/-)}$ mice, among those coupled cells, 27% were GFP^+ (Figures 3A and 3C, white arrows indicate some examples), i.e., oligodendrocytes (versus 55% in control mice). In dko mice, no coupled GFP^+ cells were seen, i.e., oligodendrocytes were completely uncoupled.

Next, we investigated whether, in Cx32/Cx47 dko mice, the protection of fPSP activity during EGD through glucose filling of astrocytes was affected. In these mice, Cx47-positive cells never colocalized with the astrocytic marker SR101 (Nimmerjahn et al., 2004; Kafitz et al., 2008) (not shown). Thus, astrocytes were identified as non-fluorescent cells with passive membrane currents and very low input resistance (1.8 ± 0.3 MΩ; n = 6, N = 6). In addition, the cell was filled with sulforhodamine B (10 μg/mL) to visualize coupling online and to ensure that the patched cell was an astrocyte. In Cx32/Cx47 dko mice, filling of an astrocyte (20 min) with glucose (20 mM) did not rescue fPSP amplitudes during EGD (light gray, 53.8% ± 6.4%, N = 6) compared with control experiments (dark gray, 46.6% ± 5.1%, N = 5) (Figure 3B, p = 0.87). These values were also similar to the fPSP decline during EGD in hGFAP-EGFP mice (orange bar in Figure 3B was taken from Figure 2C for comparison, p = 0.99 and 0.68, respectively).

Rescue of fPSPs during EGD through intercellular glucose provision is sensitive to the activity of glucose and monocarboxylate transporters

We next asked which glial and neuronal transporters participate in the rescue of synaptic activity in the thalamus. Therefore, EGD, filling of an astrocyte with glucose, and fPSP recording were performed while inhibiting glucose and monocarboxylate transporters. First, we co-applied AR-C155858 (1 μM; inhibits monocarboxylate transporters MCT1 in oligodendrocytes and MCT2 expressed by neurons) and Stf31 (5 μM; blocks glucose transporter GLUT1 expressed by astrocytes and oligodendrocytes). Under those conditions, no rescue of fPSPs during EGD was observed when filling an astrocyte with high glucose (Figure 4A, dark green bar, N = 6) because the fPSPs declined to a similar extent as that without intracellular glucose provision (to 45% ± 8% and 45% ± 5%; orange bar taken from Figure 2C, p = 0.99). Co-application of AR-C155858 and Stf31 in control ACSF (i.e., with glucose) moderately reduced fPSPs (p = 0.0145) (Figure 4B, brown, N = 7). This inhibition was significantly less compared with EGD experiments in which those blockers were applied after filling an astrocyte with glucose (73% ± 4% versus 45% ± 8%, p = 0.014). SR13800 (0.01 μM), an MCT1-specific inhibitor, did not affect fPSPs during EGD while glucose

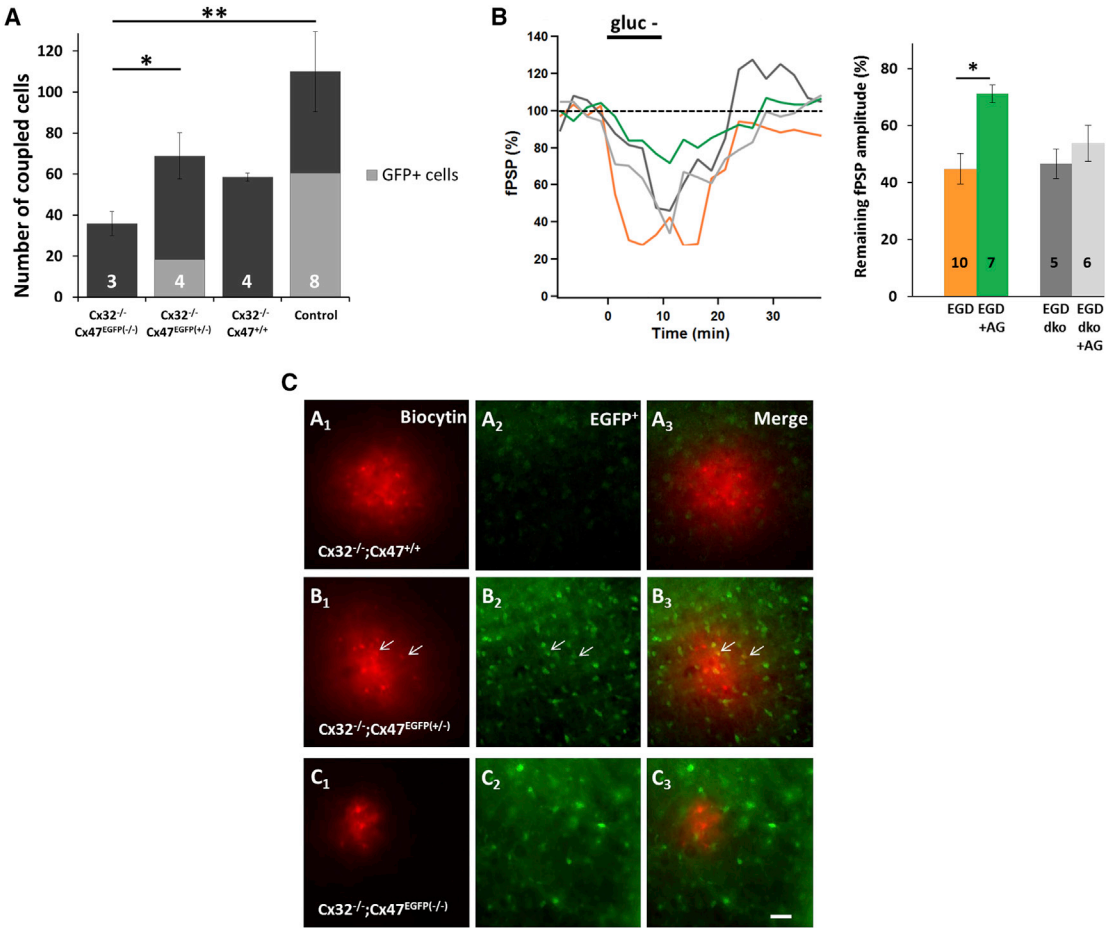

Figure 3. In Cx32/Cx47 dko mice, glucose filling of an astrocyte does not rescue the EGD-mediated decline of thalamic fPSPs

(A) Quantification of coupling efficiency in different mouse genotypes after filling SR101$^+$ thalamic astrocytes with biocytin (20 min). Total numbers (black bars) as well as the numbers of GFP$^+$ oligodendrocytes (gray bars) among all biocytin-coupled cells were compared. In Cx32$^{-/-}$;Cx47$^{EGFP(-/-)}$ (dko) mice (n = 10, N = 3), the remaining small networks completely lacked oligodendrocytes; they were used for further experiments. As expected, significantly smaller biocytin-positive networks were observed in Cx32/Cx47 dko mice compared with that of Cx32$^{-/-}$;Cx47$^{EGFP(+/-)}$ (n = 11, N = 4) and control (n = 14, N = 8) mice, with the latter containing 27% and 55% oligodendrocytes, respectively. In Cx32$^{-/-}$;Cx47$^{+/+}$mice, the proportion of oligodendrocytes was not determined because they were not fluorescent (n = 15, N = 4). The number of mice is given in the bar graphs, and error bars represent SEM. Kruskal-Wallis test followed by Dunn's test. For comparison, the control data were obtained from Griemsmann et al. (2015).

(B) Representative traces of fPSP changes during EGD in hGFAP-EGFP (EGD, orange; n = 12, N = 10) and in Cx32/Cx47 dko mice (EGD dko, dark gray; n = 5, N = 5). In addition, fPSP changes during EGD after prior filling of an astrocyte with glucose in hGFAP-EGFP (20 mM EGD+AG, green; n = 7, N = 6) and in Cx32/Cx47 dko mice (EGD dko+AG, light gray; n = 6, N = 6) are shown. Loading an astrocyte with glucose in Cx32/Cx47 dko mice did not attenuate the EGD-mediated decline of fPSPs. The number of mice is given in the bar graphs, and error bars represent SEM. ANOVA followed by Tukey's post hoc test. *p < 0.05.

(C) Immunostaining of SR101$^+$ astrocytes filled with biocytin for 20 min in the thalamus of three different genotypes: Cx32$^{-/-}$;Cx47$^{+/+}$ (A1–A3), Cx32$^{-/-}$;Cx47$^{EGFP(+/-)}$ (B1–B3), and Cx32$^{-/-}$;Cx47$^{EGFP(-/-)}$ (C1–C3). Cx47-EGFP-fluorescent oligodendrocytes are displayed in green (B2–C2), and the merged images are shown (A3–C3). Note that EGFP is not expressed in the Cx32$^{-/-}$;Cx47$^{+/+}$ mice (A2). Immunostaining for GFP (B2 and B3) revealed biocytin spread into Cx47-EGFP-fluorescent oligodendrocytes in the Cx32$^{-/-}$;Cx47$^{EGFP(+/-)}$ mice, as indicated by the co-localization of both markers (yellow cells, white arrow, B3). Scale bar, 40 μm.

filling (dark purple, N = 6) compared with EGD-only or EGD+AG (Figure 4C, p = 0.38 and 0.64, respectively). Similarly, although loading an astrocyte with glucose, AR-C155858 (light pink, n = 6) and Stf31 (light purple, N = 6) alone also failed to affect fPSPs during EGD (p = 0.21 and 0.20) or EGD+AG (p = 0.84 and 0.87, respectively) (Figure 4C). In conclusion, both MCT1/2 and GLUT1 transporters are involved in the rescue of synaptic activity when providing energy substrates through the coupled panglial thalamic network.

Finally, we asked whether, in mice lacking astrocyte gap junction coupling (Cx30$^{-/-}$;Cx43$^{fl/fl}$:hGFAPCre (DKO) mice; Wallraff et al., 2006), the protection of fPSP activity during EGD through glucose filling of oligodendrocytes was still affected. In those mice, SR101 was used to label astrocytes in the slices, and oligodendrocytes were identified as SR101-negative cells with typical passive membrane current patterns. In addition, the selected cells were dye coupled as evidenced online by adding sulforhodamine B to the pipette solution. We found that, in the

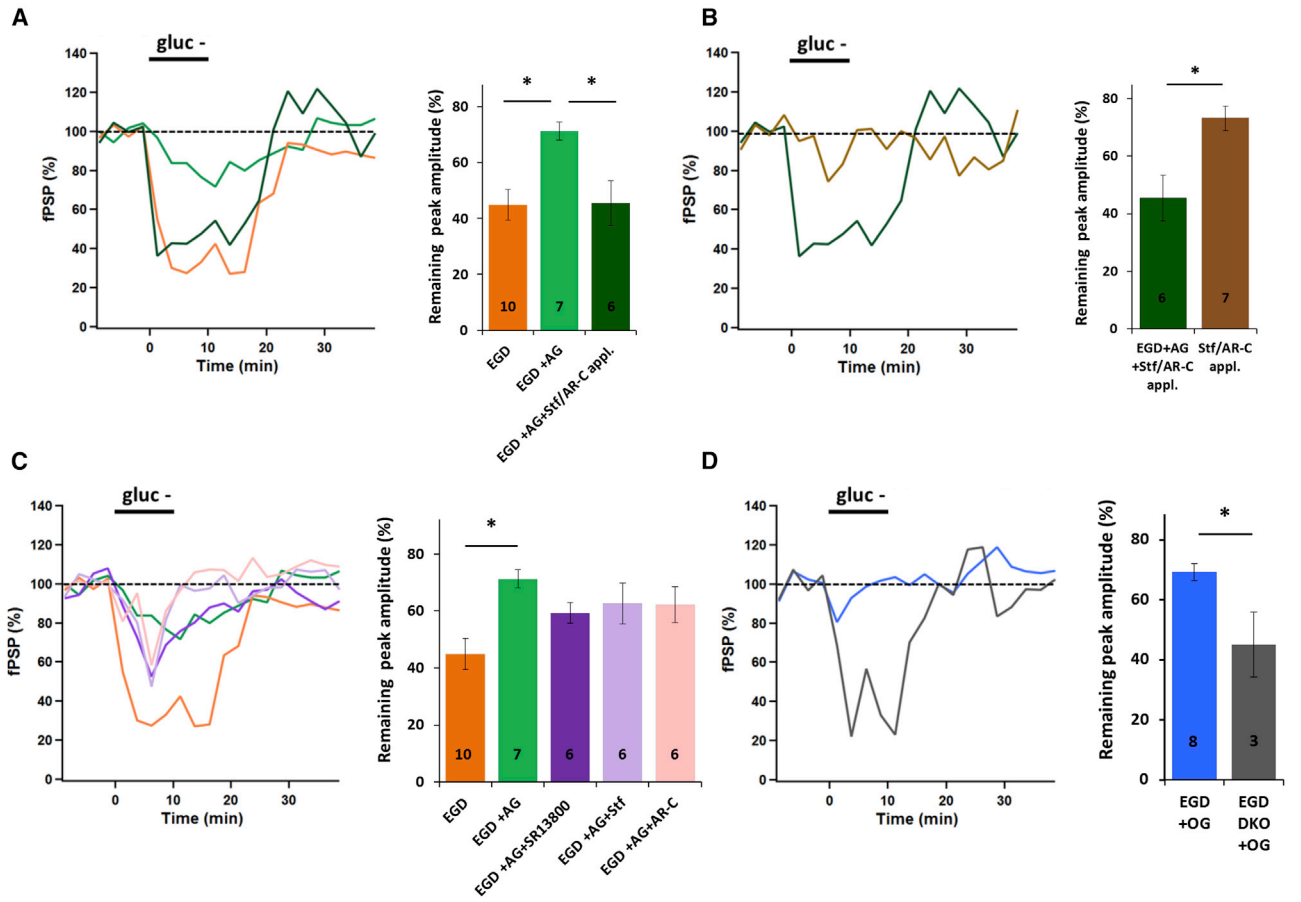

Figure 4. Simultaneous inhibition of glucose and monocarboxylate transport precludes the rescue of synaptic activity upon astrocyte glucose loading

(A) Representative traces of fPSP changes (left) and remaining fPSP amplitudes (right) during EGD in hGFAP-EGFP mice (EGD, orange, n = 12, N = 10) after filling a fluorescent astrocyte with glucose (20 mM, EGD+AG, green, n = 7, N = 6), or after filling an astrocyte with glucose (20 mM) and applying Stf-31 (5 μM) and AR-C155858 (1 μM) to block GLUT1, MCT1, and MCT2 (EGD+AG+Stf/AR-C appl., dark green, n = 6, N = 6). In the latter case, the rescue of fPSPs was abolished. Error bars represent SEM.

(B) Representative traces of fPSP changes (left) during a 10-min co-application of Stf31 and AR-C155858, when glucose was continuously perfused (Stf/AR-C appl., brown, n = 8, N = 7) and during EGD after filling an astrocyte with glucose (20 mM, EGD+AG+Stf/AR-C appl., dark green, n = 6, N = 6). The application of both blockers led to a moderate decrease in fPSPs, which was significantly lower compared with EGD experiments in which the rescue of fPSPs was abolished when those blockers were applied after loading an astrocyte with glucose (right). Error bars represent SEM.

(C) Representative traces of fPSP changes (left) obtained after filling an astrocyte with glucose (20 mM) when the MCT1-specific blockers SR13800 (0.01 μM), AR-C155858 (1 μM), or Stf-31 (5 μM) were applied (EGD+AG+SR13800, purple, n = 6, N = 6; EGD+AG+STf, light purple, n = 7, N = 6; EGD+AG+AR-C, light pink, n = 8, N = 6). None of those blockers alone affected the loss of fPSPs during EGD or EGD+AG (right). Error bars represent SEM.

(D) Representative traces of fPSP changes (left) during EGD after previous filling of an oligodendrocyte with glucose in hGFAP-EGFP (20 mM, EGD+OG, dark blue; n = 9, N = 7) or Cx30/Cx43 DKO (EGD DKO + OG, dark gray; n = 3, N = 2) mice. The histogram (right) compares fPSPs remaining under the respective conditions, normalized to the amplitudes before EGD. Note that loading an oligodendrocyte in the Cx30/Cx43 DKO mice did not attenuate the EGD-mediated decline of fPSPs. Error bars represent SEM.

The number of mice is given in bar graphs, except for (D), in which the number of slices is given. ANOVA followed by Tukey's post hoc test or t test (B and D). *$p < 0.05$.

absence of astrocyte coupling, filling of oligodendrocytes (20 min) with glucose (20 mM) failed to rescue fPSP amplitudes during EGD (dark gray, 45.1% ± 10.8%, n = 3, N = 2, p = 0.26; Figure 4D).

DISCUSSION

In the hippocampus, glial gap junction networks enable trafficking of energy metabolites to maintain glutamatergic synaptic activity (Rouach et al., 2008). These networks are almost exclusively formed by astrocytes expressing Cx43 (Griemsmann et al., 2015). In contrast, in the corpus callosum, panglial networks are dominated by oligodendrocytes (Meyer et al., 2018), indicating that glial properties are heterogeneous across brain areas (Xin and Bonci, 2018; Matyash and Kettenmann, 2010). The molecular and functional characteristics of astrocytes in the thalamus also show distinct features and thus differ from those of other regions, e.g., the hippocampus or neocortex. Thalamic astrocytes

mainly express Cx30 instead of Cx43 and lack most of the "classical" astroglial markers, such as GFAP and ALDH1L1. Notably, thalamic networks of coupled glial cells are equally composed of astrocytes and oligodendrocytes (Höft et al., 2014; Griemsmann et al., 2015; Claus et al., 2018). We, therefore, addressed the question of whether oligodendrocytes within the thalamic panglial network are needed for the provision of energy substrates to maintain neuronal activity.

The thalamus is a brain region of high energy consumption (Gordji-Nejad et al., 2018), probably also because of its long-range signaling pathways and metabolic needs for myelination. After having established a method to quantify post-synaptic network activity in slices from the ventrobasal thalamus, we investigated whether extracellular glucose can be replaced by lactate or pyruvate to maintain fPSPs. Indeed, several recent studies, mainly in the optic nerve, but also in spinal cord, have demonstrated that delivery of these substrates by oligodendrocytes is critical for axonal function (Hirrlinger and Nave, 2014; Fünfschilling et al., 2012; Brown et al., 2003; Lee et al., 2012). On the other hand, astrocytes have been shown to produce lactate, either from glucose or glycogen, and to deliver it to neurons through the astrocyte-neuron lactate shuttle (ANLS) (Pellerin and Magistretti, 2012). Thus, oligodendrocytes in the thalamic network might help sustain presynaptic function, whereas astrocytes through the ANLS might supply post-synaptic elements with energy. We found that EGD-induced decreases in fPSPs could not be prevented by extracellular lactate or pyruvate. Similar observations were made in the corpus callosum (Meyer et al., 2018), whereas, in the optic nerve, lactate may replace glucose to preserve axonal function (Brown et al., 2003). Compared with the hippocampus (Rouach et al., 2008), fPSPs declined much faster after onset of EGD, which might indicate a higher energy consumption in the thalamus because of structural differences between both regions (*cf.* above). During metabolic challenges, astrocytes may also deliver lactate derived from glycogen (Pellerin and Magistretti, 2012), and lower glycogen storage would entail a faster decline of energy reserves for neurons. Indeed, regional differences in metabolic roles imposed by astrocytes have been reported. Inhibition of glutamine synthetase led to massive glycogen accumulation in astrocytes of the hippocampus and neocortex but not in the thalamus (Yamamoto et al., 1989). Evidence for regional differences in glycogen content came from a recent immunohistochemical study revealing much lower glycogen labeling in astrocytes of the thalamus compared with other brain regions. Thus, the rapid fPSP decline during EGD in the thalamus might reflect lower glycogen reserves of those astrocytes (Oe et al., 2016).

Next, we investigated whether loading the panglial coupling network with energy substrates rescued the EGD-induced fPSP decline. We are aware that the loaded glucose concentration of 20 mM is much higher than the physiological condition. However, we assumed that there is considerable decay from the concentration in the pipette into the loaded astrocyte and, even more so, into the coupled network because of diffusion resistance. For better comparison, we used the same experimental conditions as those for the corresponding analyses in the corpus callosum (Meyer et al., 2018). Filling glucose or lactate into a single astrocyte largely prevented the decline of synaptic activity during EGD. Filling individual oligodendrocytes with the substrates had a similar effect, suggesting that the panglial networks use both astrocytes and oligodendrocytes to transport energy metabolites from blood vessels to thalamic neurons. To further substantiate a role for oligodendrocytes in sustaining synaptic activity, mice with genetic deletion of Cx32 and Cx47 were employed. These connexins are crucial for proper central myelination and oligodendrocytic coupling (Menichella et al., 2003; Odermatt et al., 2003; Maglione et al., 2010; Griemsmann et al., 2015). As expected, mice devoid of both connexins showed complete lack of oligodendrocyte coupling. Filling an astrocyte with glucose in those double-deficient mice could not rescue fPSPs during EGD. Thus, oligodendrocytes are key elements of the panglial networks for the proper neuronal energy supply in the thalamus.

Based on findings from the hippocampus, optic nerve, and corpus callosum, one may speculate that astrocytes support neurons at the synapse, whereas oligodendrocytes support them at the axons. Our stimulation paradigm includes both elements, action potential propagation via axons and synaptic transmission, and one may assume that these two glial cell types subdivide their task in supporting the neuron.

In the optic nerve, axonal activity provokes glucose uptake into oligodendrocytes through incorporation of GLUT1 into the oligodendrocytic membrane, a mechanism not requiring gap junction coupling but NMDA receptors (Saab et al., 2016). In contrast, the neuronal energy supply in the thalamus was disturbed in mice with coupling-deficient oligodendrocytes. Even though we still don't know whether thalamic oligodendrocytes lack GLUT1 and/or NMDA receptors, these finding add to the emerging view that the properties of glial cells in the thalamus are distinct from those of other brain regions (Claus et al., 2018; Griemsmann et al., 2015). Oligodendrocytes in the optic nerve show lower coupling efficiency (Butt and Ransom, 1989) and obviously have developed alternative strategies to fuel neurons.

According to the ANLS hypothesis, glucose can be taken up by astrocytes from blood vessels via GLUT1 (Bélanger et al., 2011; Barros and Deitmer, 2010). Astrocytes convert glucose into lactate and export it via MCT4 (Rafiki et al., 2003; Rinholm et al., 2011). MCT1 is expressed by oligodendrocytes and predominantly localized to the myelin sheaths around axons. Lactate can then be taking up by MCT2 to pre- or post-synaptic neurons (Pierre and Pellerin, 2005; Lee et al., 2012). In the corpus callosum, oligodendrocyte-derived glucose, rather than lactate, contributes to metabolic support of axons (Meyer et al., 2018). We applied inhibitors of GLUT1 and MCT1/2 to reveal whether panglial fueling of neurons in the thalamus involves pre-synaptic or post-synaptic mechanisms or both. Simultaneous blockage of MTCs and GLUT1 completely abolished the rescue of fPSPs observed upon astrocyte glucose loading during EGD. In contrast, the effect of blocking only GLUT1 or MCT1/2 alone, as well as the effect of SR13800, an MCT1-specific blocker, was difficult to interpret because the remaining amplitude was not different from the control situation (EGD).

To further discern how oligodendrocytes exert their effect on fPSP rescue during EGD, mice with genetic deletion of Cx30 and Cx43, in which astrocytes are completely uncoupled, were

employed (Wallraff et al., 2006). Filling an oligodendrocyte with glucose in those mice did not rescue fPSPs during EGD, suggesting that oligodendrocytes within the panglial network exert their protective effects mainly by assisting metabolite transport of astrocytes to the postsynapes, although further experiments are needed to finally resolve that issue.

Taken together, we show that astrocytes and oligodendrocytes in the thalamus are jointly engaged in maintaining synaptic activity by delivery of metabolites through the panglial-coupled network (Morrison et al., 2013). The underlying mechanisms are clearly different from other gray and white matter regions of the brain. Our data support the view that thalamic oligodendrocytes exert their effect mainly by assisting metabolite transport of astrocytes to the postsynapse, rather than by fueling axons or pre-synaptic structures.

STAR★METHODS

Detailed methods are provided in the online version of this paper and include the following:

- KEY RESOURCES TABLE
- RESOURCE AVAILABILITY
  - Lead contact
  - Materials availability
  - Data and code availability
- EXPERIMENTAL MODEL
  - Mice
- METHOD DETAILS
  - Slice preparation
  - Post-synaptic field potentials and data analysis
  - Extracellular glucose deprivation (EGD)
  - Patch-clamp recordings
- QUANTIFICATION AND STATISTICAL ANALYSES
  - Quantification of tracer coupling
  - Statistics

ACKNOWLEDGMENTS

We thank Thomas Erdmann for excellent technical assistance. This work was supported by DFG (STE 552/4 and KE329/28).

AUTHOR CONTRIBUTIONS

Conceptualization, C.S. and H.K.; Methodology, C.P. and S.G.; Investigation, C.P., and S.G.; Software, R.J.; Supervision, R.J., G.S., H.K., and C.S.; Writing – Original Draft, C.P., R.J., G.S., H.K., and C.S.; Writing – Review & Editing, C.P., R.J., S.G., H.K., and C.S.; Funding Acquisition, C.S. and H.K.

DECLARATION OF INTERESTS

The authors declare no competing interests.

Received: October 24, 2019
Revised: October 23, 2020
Accepted: December 21, 2020
Published: January 19, 2021

REFERENCES

Barros, L.F., and Deitmer, J.W. (2010). Glucose and lactate supply to the synapse. Brain Res. Brain Res. Rev. *63*, 149–159.

Bedner, P., Steinhäuser, C., and Theis, M. (2012). Functional redundancy and compensation among members of gap junction protein families? Biochim. Biophys. Acta *1818*, 1971–1984.

Bélanger, M., Allaman, I., and Magistretti, P.J. (2011). Brain energy metabolism: focus on astrocyte-neuron metabolic cooperation. Cell Metab. *14*, 724–738.

Brown, A.M., Tekkök, S.B., and Ransom, B.R. (2003). Glycogen regulation and functional role in mouse white matter. J. Physiol. *549*, 501–512.

Butt, A.M., and Ransom, B.R. (1989). Visualization of oligodendrocytes and astrocytes in the intact rat optic nerve by intracellular injection of lucifer yellow and horseradish peroxidase. Glia *2*, 470–475.

Claus, L., Philippot, C., Griemsmann, S., Timmermann, A., Jabs, R., Henneberger, C., Kettenmann, H., and Steinhäuser, C. (2018). Barreloid borders and neuronal activity shape panglial gap junction-coupled networks in the mouse thalamus. Cereb. Cortex *28*, 213–222.

Crick, F., and Koch, C. (2003). A framework for consciousness. Nat. Neurosci. *6*, 119–126.

Crunelli, V., and Hughes, S.W. (2010). The slow (<1 Hz) rhythm of non-REM sleep: a dialogue between three cardinal oscillators. Nat. Neurosci. *13*, 9–17.

Fünfschilling, U., Supplie, L.M., Mahad, D., Boretius, S., Saab, A.S., Edgar, J., Brinkmann, B.G., Kassmann, C.M., Tzvetanova, I.D., Möbius, W., et al. (2012). Glycolytic oligodendrocytes maintain myelin and long-term axonal integrity. Nature *485*, 517–521.

Fuss, B., Mallon, B., Phan, T., Ohlemeyer, C., Kirchhoff, F., Nishiyama, A., and Macklin, W.B. (2000). Purification and analysis of *in vivo*-differentiated oligodendrocytes expressing the green fluorescent protein. Dev. Biol. *218*, 259–274.

Giaume, C., Koulakoff, A., Roux, L., Holcman, D., and Rouach, N. (2010). Astroglial networks: a step further in neuroglial and gliovascular interactions. Nat. Rev. Neurosci. *11*, 87–99.

Goodenough, D.A., Goliger, J.A., and Paul, D.L. (1996). Connexins, connexons, and intercellular communication. Annu. Rev. Biochem. *65*, 475–502.

Gordji-Nejad, A., Matusch, A., Li, S., Kroll, T., Beer, S., Elmenhorst, D., and Bauer, A. (2018). Phosphocreatine levels in the left thalamus decline during wakefulness and increase after a nap. J. Neurosci. *38*, 10552–10565.

Grant, E., Hoerder-Suabedissen, A., and Molnár, Z. (2012). Development of the corticothalamic projections. Front. Neurosci. *6*, 53.

Griemsmann, S., Höft, S.P., Bedner, P., Zhang, J., von Staden, E., Beinhauer, A., Degen, J., Dublin, P., Cope, D.W., Richter, N., et al. (2015). Characterization of panglial gap junction networks in the thalamus, neocortex, and hippocampus reveals a unique population of glial cells. Cereb. Cortex *25*, 3420–3433.

Hirrlinger, J., and Nave, K.A. (2014). Adapting brain metabolism to myelination and long-range signal transduction. Glia *62*, 1749–1761.

Höft, S., Griemsmann, S., Seifert, G., and Steinhäuser, C. (2014). Heterogeneity in expression of functional ionotropic glutamate and GABA receptors in astrocytes across brain regions: insights from the thalamus. Philos. Trans. R. Soc. Lond. B Biol. Sci. *369*, 20130602.

Kafitz, K.W., Meier, S.D., Stephan, J., and Rose, C.R. (2008). Developmental profile and properties of sulforhodamine 101—labeled glial cells in acute brain slices of rat hippocampus. J. Neurosci. Methods *169*, 84–92.

Lee, Y., Morrison, B.M., Li, Y., Lengacher, S., Farah, M.H., Hoffman, P.N., Liu, Y., Tsingalia, A., Jin, L., Zhang, P.W., et al. (2012). Oligodendroglia metabolically support axons and contribute to neurodegeneration. Nature *487*, 443–448.

Magistretti, P.J., Sorg, O., Yu, N., Martin, J.-L., and Pellerin, L. (1993). Neurotransmitters regulate energy metabolism in astrocytes: implications for the metabolic trafficking between neural cells. Dev. Neurosci. *15*, 306–312.

Maglione, M., Tress, O., Haas, B., Karram, K., Trotter, J., Willecke, K., and Kettenmann, H. (2010). Oligodendrocytes in mouse corpus callosum are coupled via gap junction channels formed by connexin47 and connexin32. Glia *58*, 1104–1117.

Matthias, K., Kirchhoff, F., Seifert, G., Hüttmann, K., Matyash, M., Kettenmann, H., and Steinhäuser, C. (2003). Segregated expression of AMPA-type glutamate receptors and glutamate transporters defines distinct astrocyte populations in the mouse hippocampus. J. Neurosci. *23*, 1750–1758.

Matyash, V., and Kettenmann, H. (2010). Heterogeneity in astrocyte morphology and physiology. Brain Res. Brain Res. Rev. *63*, 2–10.

Menichella, D.M., Goodenough, D.A., Sirkowski, E., Scherer, S.S., and Paul, D.L. (2003). Connexins are critical for normal myelination in the CNS. J. Neurosci. *23*, 5963–5973.

Meyer, N., Richter, N., Fan, Z., Siemonsmeier, G., Pivneva, T., Jordan, P., Steinhäuser, C., Semtner, M., Nolte, C., and Kettenmann, H. (2018). Oligodendrocytes in the mouse corpus callosum maintain axonal function by delivery of glucose. Cell Rep. *22*, 2383–2394.

Morrison, B.M., Lee, Y., and Rothstein, J.D. (2013). Oligodendroglia: metabolic supporters of axons. Trends Cell Biol. *23*, 644–651.

Nimmerjahn, A., Kirchhoff, F., Kerr, J.N., and Helmchen, F. (2004). Sulforhodamine 101 as a specific marker of astroglia in the neocortex in vivo. Nat. Methods *1*, 31–37.

Nolte, C., Matyash, M., Pivneva, T., Schipke, C.G., Ohlemeyer, C., Hanisch, U.K., Kirchhoff, F., and Kettenmann, H. (2001). GFAP promoter-controlled EGFP-expressing transgenic mice: a tool to visualize astrocytes and astrogliosis in living brain tissue. Glia *33*, 72–86.

Odermatt, B., Wellershaus, K., Wallraff, A., Seifert, G., Degen, J., Euwens, C., Fuss, B., Büssow, H., Schilling, K., Steinhäuser, C., and Willecke, K. (2003). Connexin 47 (Cx47)-deficient mice with enhanced green fluorescent protein reporter gene reveal predominant oligodendrocytic expression of Cx47 and display vacuolized myelin in the CNS. J. Neurosci. *23*, 4549–4559.

Oe, Y., Baba, O., Ashida, H., Nakamura, K.C., and Hirase, H. (2016). Glycogen distribution in the microwave-fixed mouse brain reveals heterogeneous astrocytic patterns. Glia *64*, 1532–1545.

Pellerin, L., and Magistretti, P.J. (1994). Glutamate uptake into astrocytes stimulates aerobic glycolysis: a mechanism coupling neuronal activity to glucose utilization. Proc. Natl. Acad. Sci. USA *91*, 10625–10629.

Pellerin, L., and Magistretti, P.J. (2012). Sweet sixteen for ANLS. J. Cereb. Blood Flow Metab. *32*, 1152–1166.

Pierre, K., and Pellerin, L. (2005). Monocarboxylate transporters in the central nervous system: distribution, regulation and function. J. Neurochem. *94*, 1–14.

Rafiki, A., Boulland, J.L., Halestrap, A.P., Ottersen, O.P., and Bergersen, L. (2003). Highly differential expression of the monocarboxylate transporters MCT2 and MCT4 in the developing rat brain. Neuroscience *122*, 677–688.

Rinholm, J.E., Hamilton, N.B., Kessaris, N., Richardson, W.D., Bergersen, L.H., and Attwell, D. (2011). Regulation of oligodendrocyte development and myelination by glucose and lactate. J. Neurosci. *31*, 538–548.

Rouach, N., Koulakoff, A., Abudara, V., Willecke, K., and Giaume, C. (2008). Astroglial metabolic networks sustain hippocampal synaptic transmission. Science *322*, 1551–1555.

Saab, A.S., Tzvetavona, I.D., Trevisiol, A., Baltan, S., Dibaj, P., Kusch, K., Möbius, W., Goetze, B., Jahn, H.M., Huang, W., et al. (2016). Oligodendroglial NMDA receptors regulate glucose import and axonal energy metabolism. Neuron *91*, 119–132.

Sherman, S.M., and Guillery, R.W. (2002). The role of the thalamus in the flow of information to the cortex. Philos. Trans. R. Soc. Lond. B Biol. Sci. *357*, 1695–1708.

Wallraff, A., Köhling, R., Heinemann, U., Theis, M., Willecke, K., and Steinhäuser, C. (2006). The impact of astrocytic gap junctional coupling on potassium buffering in the hippocampus. J. Neurosci. *26*, 5438–5447.

Xin, W., and Bonci, A. (2018). Functional astrocyte heterogeneity and implications for their role in shaping neurotransmission. Front. Cell. Neurosci. *12*, 141.

Yamamoto, T., Iwasaki, Y., Sato, Y., Yamamoto, H., and Konno, H. (1989). Astrocytic pathology of methionine sulfoximine-induced encephalopathy. Acta Neuropathol. *77*, 357–368.

STAR★METHODS

KEY RESOURCES TABLE

REAGENT or RESOURCE	SOURCE	IDENTIFIER
Antibodies		
Chicken anti-GFP	Abcam	Cat# ab13970; RRID: AB_300798
Streptavidin, Alexa Fluor 647 conjugate antibody	Thermo Fisher Scientific	Cat# S-21374; RRID: AB_2336066
Alexa 488 goat anti-chicken	Invitrogen	Cat# A-11039; RRID: AB_142924
Chemicals, Peptides, and Recombinant Proteins		
Tetrodoxin citrate	Abcam	Cat# 120055; CAS: 18660-81-6
Biocytin	Sigma-Aldrich	Cat# B4261; CAS: 576-19-2
Picrotoxin	Abcam	Cat# ab120315; CAS: 124-87-8
Sulforhodamine B	Sigma-Aldrich	Cat# S1402; CAS: 3520-42-1
Pyruvate	Sigma-Aldrich	Cat# SP2256; CAS: 113-24-6
Hoechst 33342	Invitrogen	Cat# H1399
AR-C155858	MedChemExpress	Cat# HY-13248; CAS: 496791-37-8
Stf31	Sigma-Aldrich	Cat# SLM1108; CAS: 724741-75-7
SR13800	Tocris	Cat# 5431; CAS: 227321-12-2
L-lactate	Sigma-Aldrich	Cat# L7022; CAS: 867-56-1
Sulforhodamine 101	Sigma-Aldrich	Cat# S7635; CAS: 60311-02-6
Experimental Models: Organisms/Strains		
Mouse: hGFAP-EGFP (Nolte et al., 2001)	Colony maintained at the facility of the University of Bonn	N/A
Mouse: PLP-GFP (Fuss et al., 2000)	Colony maintained at the facility of the University of Bonn	N/A
Mouse: Cx32/Cx47 double KO (Odermatt et al., 2003)	Colony maintained at the facility of the University of Bonn	N/A
Software and Algorithms		
ImageJ	NIH	https://fiji.sc/or https://imagej.nih.gov/ij/; RRID: SCR_002285
Igor Pro 7.0	WaveMetrics	https://www.wavemetrics.com/; RRID: SCR_000325
R v3.5.2	R Core Team	http://www.R-project.org/R; RRID: SCR_001905
LAS AF/LAS X	Leica	https://www.leica-microsystems.com/products/microscope-software/p/leica-las-x-ls/; RRID: SCR_013673
MC Stimulus II	Multi Channels Systems	https://www.multichannelsystems.com/software/mc-stimulus-ii
Tida v5.24	HEKA	https://www.heka.com/; RRID: SCR_014582
Other		
Bipolar stimulation electrode	MicroProbes for Life Science	Cat# WE3ST31.0A10

RESOURCE AVAILABILITY

Lead contact

Further information and requests for resources and reagents should be directed to, and will be fulfilled by, the Lead Contact, Christian Steinhäuser (cste@uni-bonn.de)

Materials availability

This study did not generate any unique materials. All materials needed to support the claims of the study are available commercially.

Data and code availability

The article includes all data generated or analyzed during this study. Original source data for Figures in the paper are available upon request to the Lead Contact author. No proprietary software was used in the data analysis.

EXPERIMENTAL MODEL

Mice

Experiments were performed in transgenic mice with astrocyte-specific fluorescence labeling (human glial fibrillary acidic protein-enhanced green fluorescent protein (hGFAP-EGFP); (Nolte et al., 2001), astrocyte-specific knockout of Cx43 and global deletion of Cx30 [(Cx30$^{-/-}$;Cx43$^{fl/f}$:hGFAPCre (DKO)]; (Wallraff et al., 2006) or oligodendrocyte-specific fluorescence labeling (myelin proteolipid protein-green fluorescence protein (PLP-GFP); (Fuss et al., 2000)). In Cx32/Cx47-deficient [Cx32$^{-/-}$;Cx47$^{EGFP(+/-)}$ and Cx32$^{-/-}$;Cx47$^{EGFP(-/-)}$ (dko)] mouse lines, oligodendrocytes could be identified by EGFP fluorescence as the Cx47 coding region had been replaced by cDNA encoding the enhanced variant of the green fluorescent protein (Odermatt et al., 2003). As in our previous studies (Meyer et al., 2018; Claus et al., 2018; Griemsmann et al., 2015), mice of both sexes were used for the experiments at postnatal day (p) 28-40, except DKO mice which had an age of p23-24 . Animals were kept under standard housing conditions. All experiments were carried out in accordance to local, state (Landesamt für Natur, Umwelt und Verbraucherschutz NRW) and European regulations.

METHOD DETAILS

Slice preparation

Animals were anesthetized with Isoflurane (Abbott, Wiesbaden, Germany) and killed by decapitation. The brains were then carefully removed. The midline of each hemisphere was put on a custom-made Teflon block with a 30° angle and a small piece of the dorsal part of the brain was cut off. The hemispheres were glued dorsally on a specimen holder and cut in ice cold solution containing (in mM): 87 NaCl, 2.5 KCl, 1.25 NaH_2PO_4, 25 $NaHCO_3$, 7 $MgCl_2$, 0.5 $CaCl_2$, 25 glucose, 61.3 sucrose and bubbled with carbogen (95% O_2/5% CO_2) at pH 7,4. Using a vibratome (VT1200S, Leica, Nussloch, Germany), 300 μm thick slices for post synaptic field potential recordings and 200 μm thick slices for whole-cell patch clamp experiments, were prepared containing the ventroposteromedial (VPM) and ventroposterolateral (VPL) nuclei of the thalamus. Slices were kept at 35°C for 15 min and then stored in artificial cerebrospinal fluid (ACSF) containing (in mM): 119 NaCl, 2.5 KCl, 1.3 $MgSO_4$, 2.5 $CaCl_2$, 11 glucose, 1 NaH_2PO_4 and 26.2 $NaHCO_3$, at room temperature for at least 1 h before starting the experiments. In some cases, the slices were incubated in ASCF supplemented with 1 μM sulforhodamine 101 (SR101; Invitrogen, Thermo Fisher Scientific, Darmstadt, Germany) to label astrocytes (35°C for 20 min).

Post-synaptic field potentials and data analysis

Slices were then transferred to a recording chamber and visualized using a Leica TCS SP5 confocal microscope (Leica DM6000, Leica, Mannheim, Germany) and LAS AF software. It was equipped with a Leica HCX APO L 20x 1.0 water immersion objective and differential interference contrast (DIC) optics. Slices were constantly perfused with carbogenized ACSF. To stimulate the cortico-thalamic (CT) pathway, a bipolar stimulation electrode (WE3ST31.0A10, MicroProbes for Life Science, Gaithersburg, USA) with outside diameter of 0.61 mm, tip separation of 250 μm and an impedance of 1.0 MΩ, was placed in the internal capsule. An ACSF-filled recording electrode made from borosilicate glass capillaries with an outside diameter of 2 μm (Science Products, Hofheim, Germany) and a resistance of 3-6 MΩ was located in the ventrobasal thalamus. The distance between the two electrodes was about 700 μm. The depth of the stimulation electrode was adjusted to evoke maximal responses. Electrical stimulation was achieved with a computer-controlled constant current isolated stimulator (STG2004, Multi Channels Systems, Reutlingen, Germany). Field potentials were recorded in the ventrobasal thalamus with a SEC05-LX amplifier in the bridge mode (npi electronic, Tamm, Germany) while applying trains of stimuli (duration 100 μs, 5 stimuli at 20 Hz, from 50 μA to 200 μA, every 15 s). Ten subsequent traces were averaged and used for the analysis (giving one data point every 150 s). To obtain stable responses the stimulation intensity was set to 80% of the peak amplitude. Data analysis was performed with Igor Pro software (Wave Metrics, Portland, USA).

Extracellular glucose deprivation (EGD)

For EGD experiments, slices were first incubated with ACSF (10 min) for recording baseline fPSPs. Then, glucose-free ACSF was applied for 10 min and subsequently ACSF containing glucose was reapplied for 30 min. In some experiments, glucose was replaced by L-lactate or pyruvate (both Sigma-Aldrich, St.Louis, Missouri, USA) during the 10 min EGD step. Blockers for glucose and monocarboxylate transporters (AR-C155858, MedChemExpress, Sollentuna, Sweden; Stf31, Sigma-Aldrich, St.Louis, Missouri, USA and

SR13800, Tocris Bioscience, Bristol, United Kingdom) were applied by bath perfusion during EGD. Experiments were performed at room temperature because at 35°C, EGD (duration 5-10 min) caused an irreversible fPSP decline to zero while shorter EGD durations (2.5 min) did not affect the field potential (data not shown).

Patch-clamp recordings

Whole-cell patch clamp experiments were performed on thalamic astrocytes and oligodendrocytes, which were identified based on their morphology and green fluorescence (Matthias et al., 2003; Fuss et al., 2000; Odermatt et al., 2003). Patch pipettes were pulled from borosilicate glass capillaries (Science Products, Hofheim, Germany) by a horizontal puller (DMZ Zeitz-Puller, Zeitz, Martinsried, Germany) and had a resistance of 3-6 MΩ when filled with the following intracellular solution (in mM): 100 K-gluconate, 30 KCl, 0.5 $CaCl_2$, 1 $MgCl_2$, 5 EGTA, 20 KOH, 3 Na_2-ATP, 10 HEPES, supplemented with 20 glucose or 40 L-lactate. Sulforhodamine B (10 μg/ml; Sigma-Aldrich, St.Louis, Missouri, USA) was added to the pipette solution to visualize the coupled network during recording. Patched cells were selected close to the recording electrode (maximum distance 80 μm, same depth as the recording electrode). Cells were dialyzed for 20 min with the pipette solution prior to EGD to ensure saturation of metabolites spreading in the coupled networks. Cells were clamped at −80 mV. The liquid junction potential, calculated using Clampex (−7.1 mV), was compensated online. Input and series resistance were regularly monitored applying 10 mV voltage steps. Recordings with series resistance >20 MΩ were discarded. Currents were recorded using an EPC-800 patch clamp amplifier (Heka, Lambrecht, Germany) and monitored by TIDA software (Heka). Data were filtered at 3-10 kHz and sampled at 6-30 kHz.

QUANTIFICATION AND STATISTICAL ANALYSES

Quantification of tracer coupling

Tracer-filling experiments were performed to determine the size and composition of glial networks in acute thalamic brain slices of Cx32/Cx47-defficient mice (Griemsmann et al., 2015). To identify astrocytes, 200 μm thick slices were incubated in ACSF supplemented with SR101. Currents were recorded and cells dialyzed for 20 min with intracellular solution supplemented with 0.5% biocytin. After recording, slices were fixed in 4% paraformaldehyde (PFA) in 0.1 M phosphate buffered saline (PBS), pH 7.4, overnight at 4°C and subsequently stored in PBS. Slices were permeabilized and unspecific antibody binding sites were blocked by incubating for 4 h at room temperature in PBS containing 2% Triton X-100 and 10% normal goat serum (NGS; Millipore). They were then incubated with streptavidin-Alexa Fluor 647 (1:600; Thermo Fisher Scientific) and chicken-α-GFP (1:500; Abcam, Cambridge, UK; ab13970) in PBS with NGS (2%) and Triton X-100 (0.1%) at 4°C overnight. The next day, slices were washed 3 times in PBS and incubated 2 h at room temperature with goat-α-chicken Alexa Fluor 488 (1:500; Invitrogen A11039). Slices were then washed 3 times and incubated with Hoechst (Invitrogen; 1:100 in dH_2O, 10 min). After another washing step, slices were mounted on coverslips (Aqua-Poly/Mount, Polyscience). Stacks of image planes were acquired at a 1-2 μm intervals using a confocal microscope (TCS SP8 Leica). Coupling networks were quantified by counting the total number of biocytin-filled cells through the z stacks using ImageJ software and the cell counter plugin. Counting was performed independently by two colleagues blinded to the experimental conditions, and the results were averaged.

Statistics

Data are given as mean ± standard error of the mean (SEM). N refers to the number of animals and n to the numbers of brain slices investigated. Those numbers are indicated in the figure legends or in the text. Data were tested using analysis of variance (ANOVA) followed by Tukey's test (Gaussian datasets) or the Kruskal–Wallis test followed by Dunn's test (non-Gaussian datasets). In case two groups were compared, a t-test was applied. Differences were regarded as significant at $*p < 0.05$ or $**p < 0.01$. Tests were performed with the software R (R Development Core Team, URL http://www.R-project.org).